Astrophys Space Sci (2007) 307:57–62
DOI 10.1007/s10509-006-9268-8

ORIGINAL ARTICLE

Numerical Simulations and Astrophysical Applications of Laboratory Jets at Omega

R. F. Coker · B. H. Wilde · J. M. Foster · B. E. Blue · P. A. Rosen · R. J. R. Williams · P. Hartigan · A. Frank · C. A. Back

Received: 28 April 2006 / Accepted: 17 October 2006

Abstract We have conducted experiments on the Omega laser at the University of Rochester that have produced jets of supersonic Ti impacting and being deflected by a ball of high density plastic. These mm-sized jets of dense plasma are highly complex, have large Reynolds numbers, and, given sufficient time and shear, should produce a fully turbulent flow. The experiments are diagnosed with a point-projection backlighter, resulting in a single image per shot. Simulations of the 3D hydrodynamics capture the large-scale features of the experimental data fairly well while missing some of the smaller scale turbulent-like phenomena. This is to be expected given the limited characterization of the targets as well as the finite resolution of the 3D simulations. If Euler scaling holds, these experiments should model larger astrophysical jets in objects such as HH 110 where an outflow can be seen colliding with a molecular cloud. However, Euler scaling demands that not only the isothermal internal Mach numbers of the two systems be similar but also that any dissipative mechanisms, such as radiative cooling or viscous dissipation, be of equal importance relative to each other. Similar equations of state are required as well. We discuss such issues in the context of these experiments and simulations.

Keywords Hydrodynamics · ISM: Herbig-Haro objects · ISM: Jets and outflows · Methods: Laboratory

J. M. Foster · P. A. Rosen · R. J. R. Williams
AWE, Aldermaston, Reading, UK

R. F. Coker (✉) · B. H. Wilde
Los Alamos National Laboratory, Los Alamos, NM

B. E. Blue
Lawrence Livermore National Laboratory, Livermore, CA

P. Hartigan
Department of Physics and Astronomy, Rice University, Houston, TX

A. Frank
Department of Physics and Astronomy, University of Rochester, Rochester, NY

C. A. Back
General Atomic, Inertial Fusion Group, San Diego, CA

1 Background

HH 110 (the left image in Fig. 1) is an astrophysical jet roughly a parsec in size. Our experiments on Omega (the right image in Fig. 1) are a few mm in size. What can we learn about the former from the latter? Strict scaling arguments (see below) show that under certain conditions the two systems behave the same way although they are nearly 20 orders of magnitude different in size. Thus, behavior seen in one should be applicable to the other. In addition, validation of codes used to model one system successfully should result in codes that can be applied to the other equally well; the better the scaling, the more confidence one has in applying a code to the other problem. As such, these experiments are part of a large validation program spanning many national laboratories and the astrophysical community. In this work, we focus on simulations of the LANL/SAIC code RAGE, a radiative hydrodynamics Eulerian code with continuous adaptive grid refinement that uses a Godunov scheme with implicit 2T hydrodynamics. The experiments have been very successful in that they have shown clearly what the codes can and cannot do. For example, the experiments pointed out a temporary code issue with shocks converging at $r = 0$ in RZ co-ordinates. Without detailed knowledge of initial conditions or a turbulence model, the codes do not reproduce

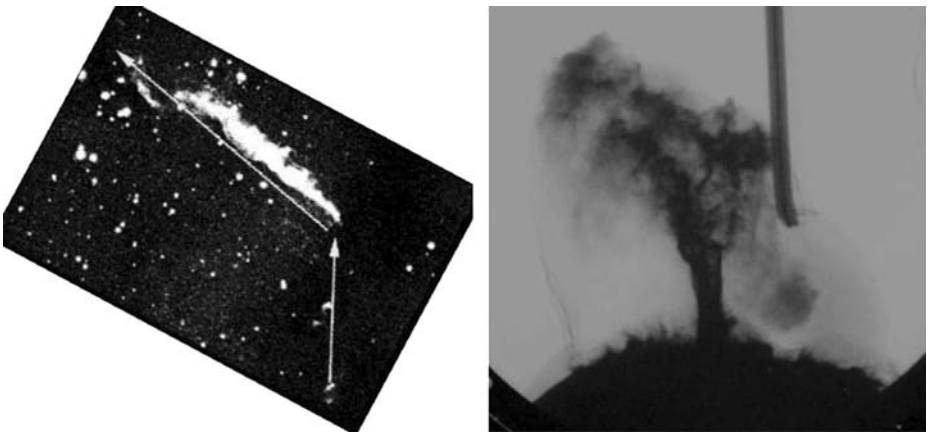

Fig. 1 Images of deflected jets. The left image is an HST observation of HH110 (Reipurth et al., 1996) while the right image is a Zn radiograph from our experiments on Omega

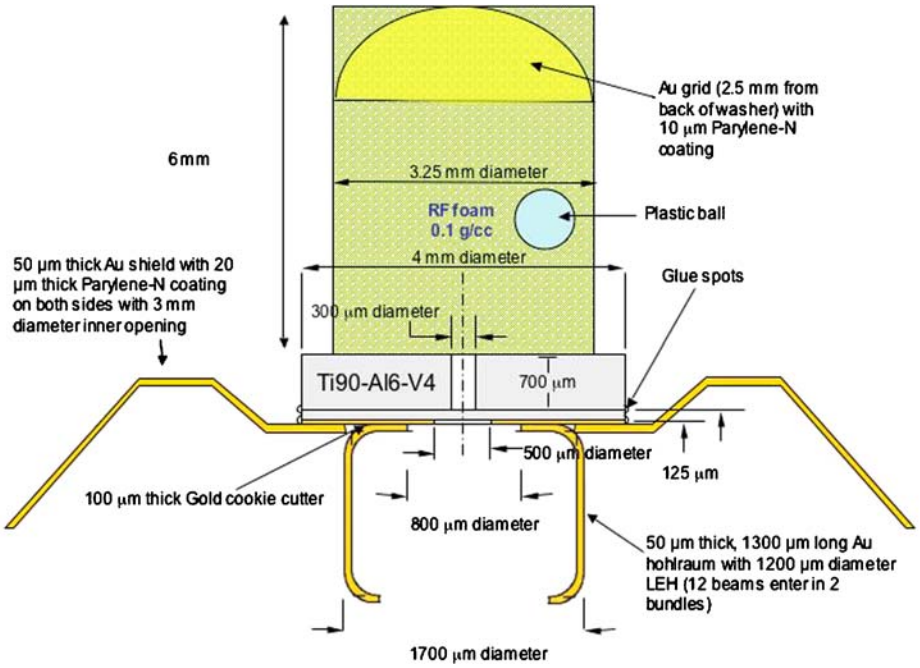

Fig. 2 The experimental setup. Lasers enter the hohlraum from below, resulting in a pressure drive on the Ti disc. A jet of Ti forms and enters the RF foam. A backlighter (not shown) perpendicular to the target is used to illuminate the foam. A transmission radiograph is then captured on film

some of the small-scale details of the experiments. However, the larger scale features are captured quite well (see below).

Figure 2 shows a schematic of the experimental setup. We use indirect drive, where a number of laser beams (here, 12 beams at 450 J each) are directed into a gold hohlraum. The laser beams radiatively ablate the gold and plasma accumulates in the hohlraum. The resulting pressure build-up in the hohlraum drives the target, a cap and washer of TiAlV alloy. A shock enters the Ti cap, breaks out into the 'free-run' region (the hole in the Ti washer), and produces a jet of material that enters a foam. A few additional laser beams are directed towards a backlighter pinhole target made of Zn (or Fe in some cases). The pinhole focuses the resulting 4 to 7 keV photons so that they illuminate the cylindrical 100 mg/cc RF target foam. Finally, a transmission radiograph image is captured on film by a camera. Each experiment or 'shot' results in a single image. A gold grid with a plastic coating is included on each shot for target registration and resolution modeling. A gold shield is used to minimize the number of photons from the drive side of the target that reach the film while a gold washer or 'cookie cutter' is included to minimize direct shocking of the Ti washer. In some shots, a normal density plastic ball is placed as in obstacle in the foam. Codes that include laser drive physics (e.g. NYM at AWE) were used to match DANTE time-resolved observations of the apparent brightness temperature of the hohlraum wall from previous experiments with a very similar drive profile (Foster et al., 2002). The profile used by RAGE in the models presented here is shown in the left plot in Fig. 3. The profile corresponds to the modeled "air" temperature (although the targets are

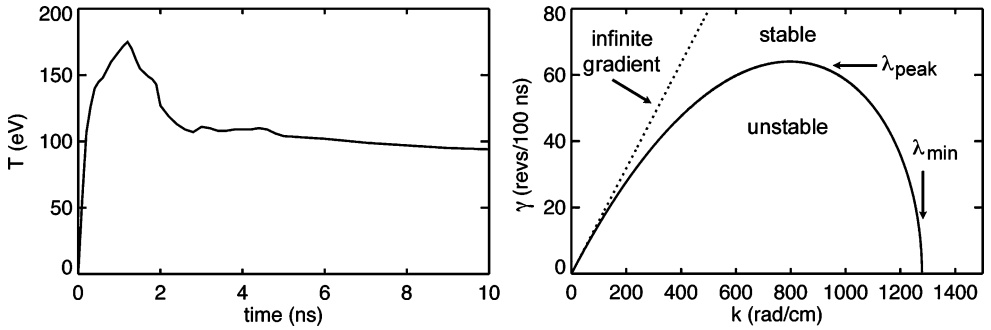

Fig. 3 A plot of the temperature profile used to drive the target (left). The nominal laser pulse is a square 1 ns pulse with a peak drive temperature of ∼180 ev. Note that the temperature source (used in the RAGE simulations) is not quite the same as the profile seen by DANTE for reasons such as hole closure (Foster et al., 2002). The right figure shows the KH instability growth rate using typical values for the experiments. Both linear (dotted) and nonlinear (solid) growth rates are shown. The wavelengths of perturbations in the targets correspond to wavenumbers (k) that are larger than the maximum unstable wavenumber so KH growth is not likely to occur

shot in a vacuum, the simulations use low-density air since RAGE requires non-zero starting densities) in the middle of the hohlraum that is required by RAGE to get the observed hohlraum wall brightness temperature.

2 Instabilities

Kelvin-Helmholtz (KH) instabilities do not appear in these experiments. If one assumes a finite velocity gradient across an interface such that over a scale δ there is a velocity change ΔV, one gets a KH growth rate like that shown in the right figure in Fig. 3. The figure shows the growth rate, in revolutions of growth per unit time, for $\delta = 5$ μm and $\Delta V = 5 \times 10^6$ cm/s, typical values for these experiments. Also shown is the linear growth rate that corresponds to an infinite velocity gradient (Chandrasekhar, 1961). The minimum wavelength ($\lambda = 2\pi/k$) required for KH growth is $\lambda_{\min} = 50$ μm while the most rapid growth occurs at $\lambda_{\text{peak}} = 80$ μm. Thus, with $\lambda_{\text{initial}} \sim 1$ μm, KH is not initially important for these experiments. Note that the wavenumber corresponding to the most rapid KH growth (∼32 revolutions of growth over the 100 ns of the experiment) is $k_{\text{peak}} = 0.64/\delta$. However, the rate of growth for Rayleigh-Taylor (RT) instabilities goes as $\sqrt{(\text{kg})} \sim 1$ rev/ns for $\lambda = 1$ μm. Since the target surface roughness is ∼1 μm, RT may be important over the hundreds of ns duration of the experiments; RT is quite possibly the cause of the 'smoke' seen in the right hand image in Figs. 1 and 5. We have run simulations that included target perturbations to investigate instability growth. To simulate burrs on the target of roughly 1 μm, since we need ∼8 cells across a feature, we require sub-micron resolution. Other 3D features, such as the offset of the Au washer relative to the free-run region, need to be included as well. Such high-resolution 3D models are not yet feasible. However, coarser 3D simulations with large ($> 10\mu$m) perturbations show that, as expected, the macroscopic features of the flow are sensitive to the initial conditions.

3 Scaling

These experiments will scale to arbitrary dimensions if the polytropic Euler equations encompass all the relevant physics:

$$\rho\left(\frac{\partial \mathbf{v}}{\partial t} + \mathbf{v}\cdot\nabla\mathbf{v}\right) = -\nabla p$$

$$\frac{\partial \rho}{\partial t} + \nabla\cdot(\rho\mathbf{v}) = 0$$

$$\frac{\partial p}{\partial t} - \gamma\frac{p}{\rho}\frac{\partial \rho}{\partial t} + \mathbf{v}\cdot\nabla p - \gamma\frac{p}{\rho}\mathbf{v}\cdot\nabla\rho = 0$$

For a given adiabatic index, γ, the Euler equations are invariant under transformations that preserve the Euler number, $\text{Eu} = v\sqrt{(\rho/P)}$, where v is a velocity, ρ is density, and P is pressure. Thus, if one assumes dissipative mechanisms (thermal diffusion, viscosity, and radiation) are negligible, the Euler equations contain all the relevant physics and the experiment can be scaled to arbitrary dimensions (Ryutov et al., 1999). The conditions for these three mechanisms to be unimportant are $vL/\kappa = \text{Pe} \gg 1$, $\rho L v/\eta = \text{Re} \gg 1$, and $v\tau/L = \chi \gg 1$, where κ is the thermal diffusivity, η is the dynamic viscosity, τ is the radiative cooling time, and L and v are some length and velocity scale, respectively. Strictly speaking, the experiment can be shown to scale even if radiation is non-negligible (Ryutov et al., 2001). Table 1 shows some characteristic values for the experiments as well as for HH 110, a Herbig-Haro object with a jet extending from a young star system and being deflected by a large molecular cloud (Riera et al., 2003). For all regions of the flow that are important, the local Reynolds number, Re, is more than 10^5, so turbulence may develop at late times if there is enough shear (Robey et al., 2003); it is not clear how fully developed turbulence affects scaling. In the experiment, which does not have a fully ionized plasma, viscosity is determined by

Table 1 List of characteristic values for the jet 'flute' and bow-shock regions of the Omega experiments and for HH 110. The local isothermal Mach number, known as the Euler number, is spatially and temporally variable in the experiments, making firm scaling to HH 110 difficult. If the functional shape of the Euler number, as a function of timescale, is the same between the experiments and HH 110, scaling will persist; otherwise, the experiments scale only for a finite time

Quantity	Symbol	Omega (core sheath)	Omega (bow-shock head)	HH 110
Temperature	T	0.1 eV	0.06 eV	8000 K
Density	ρ	3 g/cc	2 g/cc	1×10^{-21} g/cc
Pressure	P	2×10^{10} dyn/cm^2	2×10^{11} dyn/cm^2	10^{-9} dyn/cm^2
Fluid velocity	u	10 km/s	4 km/s	300 km/s
Lengthscale	L	20 μm	200 μm	500 AU
Timescale	$t = L\sqrt{(\rho/P)}$	25 ns	60 ns	50 yrs
Jet sound speed	c_s	2 km/s	4 km/s	10 km/s
Local Mach number	$M = u/c_s$	5	1	30
Kinematic viscosity	v	$\sim$0.1 cm^2/s	$\sim$0.05 cm^2/s	$\sim 10^{19}$ cm^2/s
Reynolds number	Re	$\sim 10^5$	$\sim 10^5$	$\sim 10^5$
Peclet number	Pe	$\sim 10^9$	$\sim 10^{10}$	$\sim 10^5$

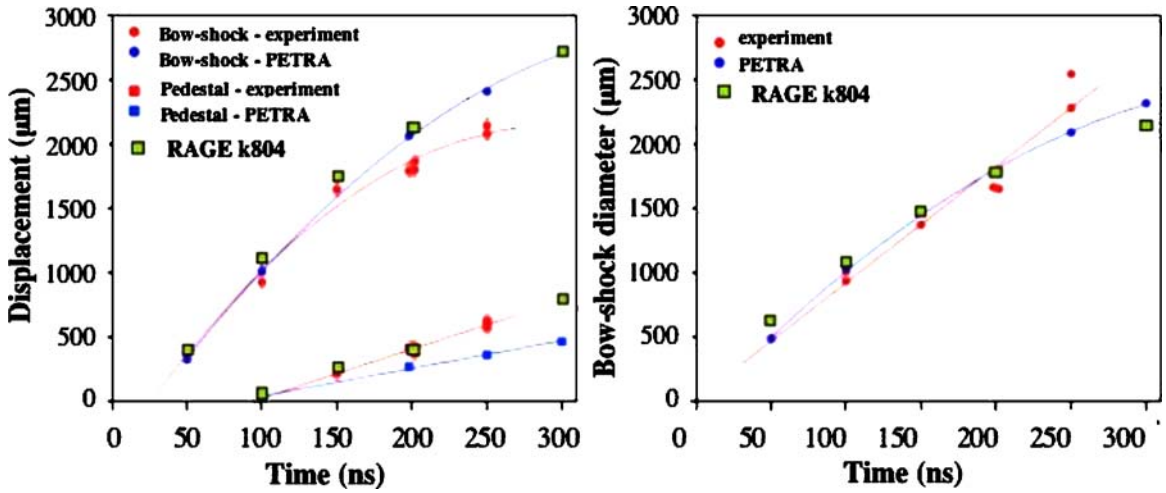

Fig. 4 Comparison of simulation (PETRA in blue and RAGE in yellow) results to the experimental data. In the left figure is displacement of the bow-shock and the 'pedestal' (the large rounded feature at the bottom of the data shown in the right image of Fig. 1). The right figure shows the comparison for the diameter of the bow-shock. Scatter in the data reflects uncertainty of initial and drive conditions

the degree of coupling between ions (Clerouin et al., 1998). In the simulations, viscosity is dominated by shock treatments so one can use the sound speed, c_s, to estimate Re by (Landau and Lifshitz, 1987) $\rho c_s \Delta_{sh}/4$. In RAGE the 5 to 95% shock width (Δ_{sh}) is $\sim$7 cells, regardless of the details of the problem, so $Re = 7/4\rho c_s \Delta x$. In that viscosity is unimportant in both cases, one must have a numerical Re which is also $\gg$1 in order for the simulations to correctly represent the experiments. To get astrophysical scaling, Re for the experiment, the simulation, and the astrophysical object all need to be $\gg$1. This holds true for these Omega experiments and for HH 110 but not for coarse resolution (10 s of μm) simulations. To get $\mathrm{Re}^{\mathrm{RAGE}} > \sim 10$ in all regions of interest, we require $\sim$1 μm resolution. Such high-resolution simulations do start to capture much of the observed 3D behavior (Foster et al., 2005). Of course, such conclusions depend on the choice of length scale; here, we are interested in the jet 'flute' and so we choose the width of that feature ($\sim$200 μm) as our scale. Re in such a case is large enough in the simulations to capture the relevant features of the experiments. Note that Euler scaling transforms time as $L\sqrt{(\rho/P)}$, so from Table 1 it can be seen that $\sim$25 ns in the experiments is equivalent to $\sim$50 yrs in HH 110. Table 1 also shows that thermal diffusion is not important in these experiments.

4 Code comparisons

Comparison of simulations by both RAGE and PETRA to data with no plastic ball is shown in Fig. 4. RAGE does slightly better than PETRA on the pedestal formation,

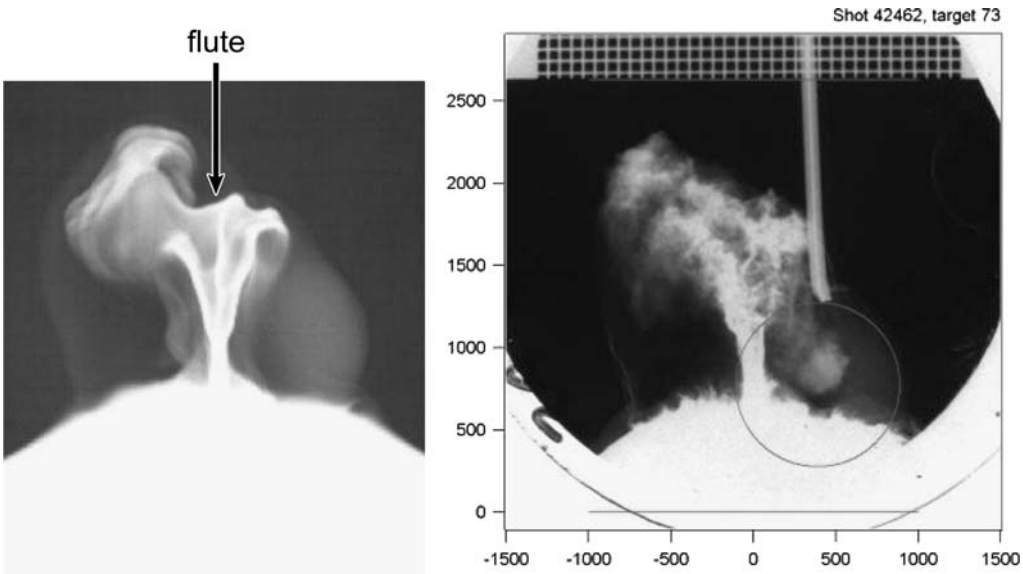

Fig. 5 Images of simulated (left) and experimental (right) radiographs. The circle shows the initial location of the plastic ball. Scale is in units of microns. The stalk holding the ball (not included in this simulation) and the Au grid can be seen. Due to the coarse 12 μm resolution, the 'grass' on the pedestal is not clearly seen in the simulations. The Y-shaped 'flute' (see Section 4) is labeled in the simulated radiograph

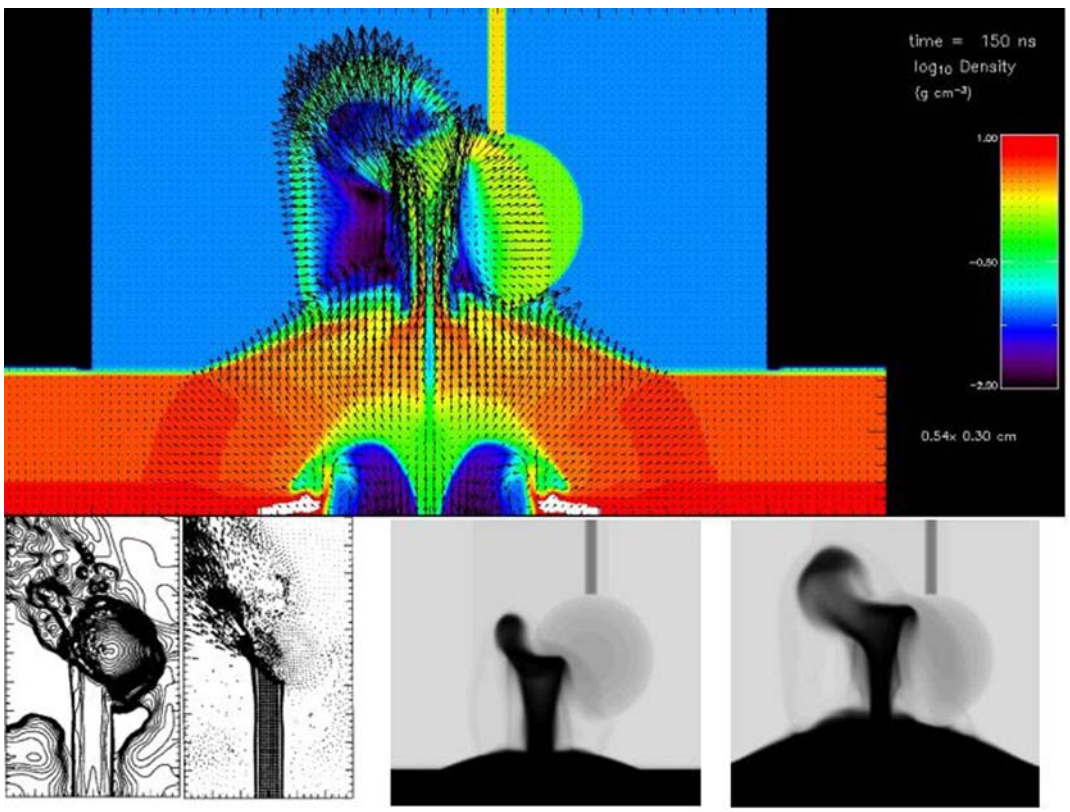

Fig. 6 Density contours and velocity vectors for simulations of HH 110 (lower left) from de Gouveia Dal Pino (1999), velocity vectors imposed over a scaled color image of density for a simulation of the Omega experiments (top), and simulated Zn radiographs at 100 (lower middle) and 150 ns (lower right)

but both codes over-predict the displacement of the bow-shock, implying the experiment has more late-time dissipation than the codes. The scatter in the experiment data, reflects shot-to-shot variability; both codes are within the scatter for the bow-shock diameter but not for the displacement of the bow-shock and the pedestal. For RAGE, new 2D to 3D linking permits better numerical resolution at early time (during ablation) to capture more of the resulting late time 3D features (such as the smoke and the grass seen in Fig. 5). Figure 5 shows a comparison of a simulated RAGE radiograph to the data. The simulation matches macroscopic features such as bow-shock location quite well. It of course does not reproduce small-scale features that are related to (unknown) details of the initial conditions. We are starting to use other codes such as FLASH (Calder et al., 2002) to model the Omega experiments. Initial hydrodynamics-only FLASH results, using a material energy source in the Ti plug, with coarse (30 μm) resolution show no fine details at the jet head but there is apparent KH behavior along the jet that is not seen in the experiments or RAGE or PETRA simulations.

Figure 6 shows a comparison of a RAGE simulation of the experiments to a simulation of HH 110 (de Gouveia Dal Pino, 1999). The images show that the coarse structure of the flow is similar for the two systems; this is expected since both are jets colliding with and being deflected by a large obstacle. However, there has been as yet no attempt to match the fine details. Figure 6 also shows images of a 3D RAGE simulation at 100 and 150 ns, illustrating how the jet evolves. Note the fairly poor resolution (higher resolution simulations show more 3D 'smoky' behavior). Observe the bow-shock in the plastic ball, the deflection of part of the jet, and the formation of the pedestal. The 'flute' formation and breakup is particularly hard to model. There is also 'grass' on the pedestal behind (or at – one cannot tell the difference in the 2D transmission image) the edge of the Mach ring. The grass is most likely debris being kicked up by the Mach ring shock traveling perpendicular to the backside of the Ti washer surface. Such features help point the way to where better physics models are required.

5 Summary

We have developed a test bed for experiments on Omega that can be scaled to astrophysical objects. Our present Omega jet experiments can be well modeled by simulations using a variety of codes. These particular experiments scale roughly to HH 110. These types of experiments help validate codes so they can then be used directly on astrophysical problems. In the future, we hope to move to a higher Mach number, a higher aspect ratio, and perhaps a radiative jet (where scaling will still apply). These experiments continue to drive code improvements as well as quantitative image analysis.

References

Calder, A.C., et al.: ApJS **143**, 201 (2002)
Chandrasekhar, S.: Hydrodynamic and Hydromagnetic Stability. Oxford Univ. Press, New York (1961)
Clerouin, J.G., Cherfi, M.H., Zerah, G.: Europhys. Lett. **42**, 37 (1998)
de Gouveia Dal Pino, E.M.: ApJ **526**, 862 (1999)
Foster, J.M., et al.: ApJ **634**, L77 (2005)
Foster, J.M., et al.: Phys. Plasmas **9**, 2251 (2002)
Landau, L.D., Lifshitz, E.M.: Fluid Mechanics, Vol. 6, Course of Theoretical Physics, 2nd ed. (1987)
Robey, H.F., et al.: Phys. Plasmas **10**, 614 (2003)
Reipurth, B., Raga, A.C., Heathcote, S.: A&A **311**, 989 (1996)
Riera, A., et al.: AJ **126**, 327 (2003)
Ryutov, D.D., et al.: ApJ **518**, 821 (1999)
Ryutov, D.D., Remington, B.A., Robey, H.F., Drake, R.P.: Phys. Plasmas **8**, 1804 (2001)